

Experimental observation of a current-driven instability in a neutral electron-positron beam

J. Warwick,¹ T. Dzelzainis,¹ M. E. Dieckmann,² W. Schumaker,³ D. Doria,¹ L. Romagnani,⁴ A. Alejo,¹ K. Poder,⁵ J. M. Cole,⁵ M. Yeung,¹ K. Krushelnick,⁶ S.P.D. Mangles,⁵ Z. Najmudin,⁵ B. Reville,¹ G. M. Samarin,¹ D. Symes,⁷ A. G. R. Thomas,^{6,8} M. Borghesi,¹ and G. Sarri^{*1}

¹*School of Mathematics and Physics, Queen's University Belfast, University Road, Belfast BT7 1NN, UK*

²*Department of Science and Technology (ITN), Linköping University, Campus Norrköping, 60174 Norrköping, Sweden*

³*SLAC National Accelerator Laboratory, Menlo Park, California 94025, USA*

⁴*LULI, Ecole Polytechnique, CNRS, CEA, UPMC, 91128 Palaiseau, France*

⁵*The John Adams Institute for Accelerator Science,*

Blackett Laboratory, Imperial College London, London SW72BZ, UK

⁶*Center for Ultrafast Optical Science, University of Michigan, Ann Arbor, Michigan 481099-2099, USA*

⁷*Central Laser facility, Rutherford Appleton Laboratory, Didcot, Oxfordshire OX11 0QX, UK*

⁸*Lancaster University, Lancaster LA1 4YB, United Kingdom*

(Dated: September 14, 2022)

We report on the first experimental observation of a current-driven instability developing in a quasi-neutral matter-antimatter beam. Strong magnetic fields (≥ 1 T) are measured, via means of a proton radiography technique, after the propagation of a neutral electron-positron beam through a background electron-ion plasma. The experimentally determined equipartition parameter of $\epsilon_B \approx 10^{-3}$, is typical of values inferred from models of astrophysical gamma-ray bursts, in which the relativistic flows are also expected to be pair dominated. The data, supported by Particle-In-Cell simulations and simple analytical estimates, indicate that these magnetic fields persist in the background plasma for thousands of inverse plasma frequencies. The existence of such long-lived magnetic fields can be related to analog astrophysical systems, such as those prevalent in lepton-dominated jets.

PACS numbers: 52.27.Ep, 52.35.Qz, 98.62.Nx

The exact symmetry between its positively and negatively charged constituents makes electron-positron beams (EPBs) a unique case in plasma physics. Besides the fascinating fundamental implications of this complete symmetry, EPBs are currently believed to play a central role in a range of high-energy astrophysical phenomena, such as the ultra-relativistic outflows from active galactic nuclei and pulsars [1–4]. It has been proposed that pair-dominated jets might play a role in the emission of Gamma-Ray Bursts (GRBs), produced in compact object (black hole or neutron star) mergers/collisions, or during the death of massive stars. These events account for some of the most luminous events in the universe [5, 6].

Arguably, the most fundamental open question regarding EPBs in astrophysical systems concerns their interaction with the ambient environment, and in particular the related growth of plasma instabilities [7–9], an essential ingredient in the formation of collisionless shocks and their radiative emission [10, 11]. These phenomena require magnetic energy densities with values greatly exceeding that of the ambient plasma (typically with a mean field on the order of a nT [12]). In these scenarios, the strength of the magnetic fields is usually given in terms of the so-called equipartition parameter $\epsilon_B = U_B/U_e$, with $U_B = B^2/2\mu_0$ and $U_e = \gamma_b n_b m_e c^2$ the magnetic and total kinetic energy density, respectively (here n_b and γ_b refer to the density and bulk Lorentz fac-

tor of the beam or shock, respectively). Analysis of GRB afterglow spectra indicates that they must be the result of synchrotron radiation in a magnetic field with typical values of ϵ_B ranging from 10^{-5} [13, 14] to 0.1 [15, 16]. These values cannot be obtained by MHD shock compression of the local magnetic fields ($\epsilon_B \approx 10^{-11}$ [17]) or by magnetic flux carried from the central engine ($\epsilon_B < 10^{-7}$ [18]). Weibel-mediated shocks in the jet could generate fields of sufficient strength, but are expected to decay rapidly, on timescales comparable to the inverse plasma frequency [11]. On the other hand, analytical [8] and numerical [19–22] studies give significant evidence that magnetic fields of sufficient strength and persistence might be generated by strong current filamentation of the EPB.

Despite the central role of such a mechanism in these phenomena, there is no direct evidence of its existence, either in the laboratory or in astrophysical observations. These theories thus currently lie beyond experimental validation, even though it is possible to rescale these phenomena down to laboratory size plasmas [23]. Advancing previous efforts in the area [24–26], it is a relatively recent development that high density electron-positron beams can be generated in the laboratory [27, 28] in a fully laser-driven setup [29]. Under optimum conditions, a quasi-neutral electron-positron beam can be generated [27], with a broad spectrum and a divergence of the order of tens of milliradians [28].

In this Letter, we show experimentally that the prop-

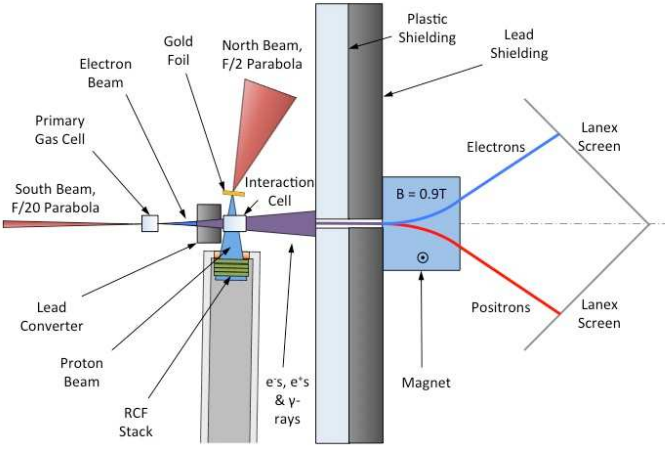


Figure 1. Sketch of the experimental setup.

agation of such an EPB through a background electron-ion plasma can generate a strong and long-lived magnetic field, as a result of a current-driven beam-plasma instability. The field, detected via a proton imaging technique [30, 31], persists for at least $(2.5 \pm 0.5) \times 10^3$ inverse plasma frequencies of the background plasma (temporal window of the observation), without significantly changing its amplitude and spatial extent. The measured amplitude of 1.2 ± 0.5 T implies an equipartition parameter $\epsilon_B \approx 10^{-3}$, in line with what predicted for astrophysical jets. The present experiment relates to a fundamental mechanism thought to play a central role in the dynamics of astrophysical jets interacting with the ambient medium.

The experiment was carried out using the Astra-Gemini laser [32] hosted by the Central Laser Facility at the Rutherford Appleton Laboratory, UK. The experimental setup is sketched in Fig. 1. A short (pulse duration of 45 ± 2 fs) laser pulse, containing an energy of approximately 9 J, was focussed, using an F/20 off-axis parabola, down to a focal spot of diameter 27 ± 5 μm at the entrance of a 10mm-long gas-cell filled with a He gas doped with 3% of N_2 . The helium gas was fully ionized by the laser pulse, producing a plasma density of $4 \times 10^{18} \text{ cm}^{-3}$, measured by optical interferometry. The interaction generated, via laser-wakefield acceleration [33], a reproducible electron beam with a broad spectrum extending to approximately 600 MeV and an overall charge of the order of 0.40 ± 0.04 nC (similar to what reported in Re. [27]). The laser power and gas density were chosen in order to stay slightly above the threshold for ionisation injection [34]. The electron beam then interacted with a thick lead target with a variable thickness (ranging from 5 to 25mm) in order to generate an EPB that subsequently propagated through a secondary gas-cell filled with pure He. By changing the thickness of the converter target, the percentage of positrons in the

EPB can be controlled, seamlessly, from 0% to approximately 50% [27]. A magnetic spectrometer was placed downstream of the interaction to separate and measure the spectrum of the electrons and positrons in the beam. This spectrometer consisted of a 10cm long, 0.8T dipole magnet followed by two LANEX stintillator screens.

A second laser pulse (pulse duration of 45 ± 2 fs and energy of 9J) was focussed, using an F/2 off-axis parabola, on the surface of a $20\mu\text{m}$ thick gold foil in order to generate, via Target Normal Sheath Acceleration [35], a multi-MeV proton beam (cut-off energy of $\simeq 5$ MeV) that was used to probe the interaction gas-cell, transverse to the EPB propagation. The proton beam was then recorded by a stack of RadioChromic Films (RCF) [36], providing spatially and temporally resolved measurements of the fields left in the plasma with a geometrical magnification $M \approx 8$ [30]. In this manuscript we focus our attention on radiographs of the same interaction obtained with proton energies of 4.5, 3.3, and 1.1 MeV (each with an uncertainty of 0.5 MeV [30]). These energies correspond to probing the background plasma (14 ± 6) ps, (60 ± 10) ps, and (280 ± 30) ps after the arrival of the EPB. For a converter thickness of 2.5 cm (corresponding to approximately 5 radiation lengths), an EPB with $N_e = (3.2 \pm 0.3) \times 10^9$ electrons, $N_p = (3.0 \pm 0.2) \times 10^9$ positrons (positrons accounting for $48 \pm 5\%$ of the overall leptonic beam), an inferred beam duration at source of the order of $\tau_b \approx 100$ fs, a divergence of the order of 30 - 50 mrad, and a source size of the order of 300 μm , was consistently generated (analogous to Ref. [27]). Moreover, electrons and positrons presented a broad spectrum well approximated by a Jüttner-Synge distribution (average Lorentz factor $\gamma_b \approx 15$). The number density of the EPB at the entrance of the second gas-cell, placed 7 mm away from the rear surface of the converter target, is $n_b = (2.6 \pm 0.5) \times 10^{14} \text{ cm}^{-3}$. The EPB co-propagated with an intense burst of bremsstrahlung γ -rays as modelled by Monte-Carlo simulations using the nuclear scattering code FLUKA [37]. Hydrodynamic simulations (using the commercial code HYADES [38]) indicate that this photon beam fully ionised the He gas in the second gas-cell to an average electron density of $n_{\text{pl}} = 10^{17} \text{ cm}^{-3}$ (corresponding electron plasma frequency $\omega_{\text{pl}} \approx 2 \times 10^{13} \text{ Hz}$) and a temperature of the order of 10 eV.

Fig.2 shows typical radiographs of the He plasma after the propagation of an EPB with different percentages of positrons (from 23%, frame a., to 48%, frame c.). In all cases the electron density of the background gas was kept constant to a value of $n_{\text{pl}} \approx 10^{17} \text{ cm}^{-3}$. For a low percentage of positrons (frame a.) no proton deflections are observed, with the probing proton beam retaining a smooth spatial profile. As the positron percentage in the EPB is increased (thicker converter target, see Ref. [27]) a faint modulation starts to be observed along the vertical axis (frame b.), which becomes apparent whenever the EPB approaches overall charge neutrality (frame c.). In

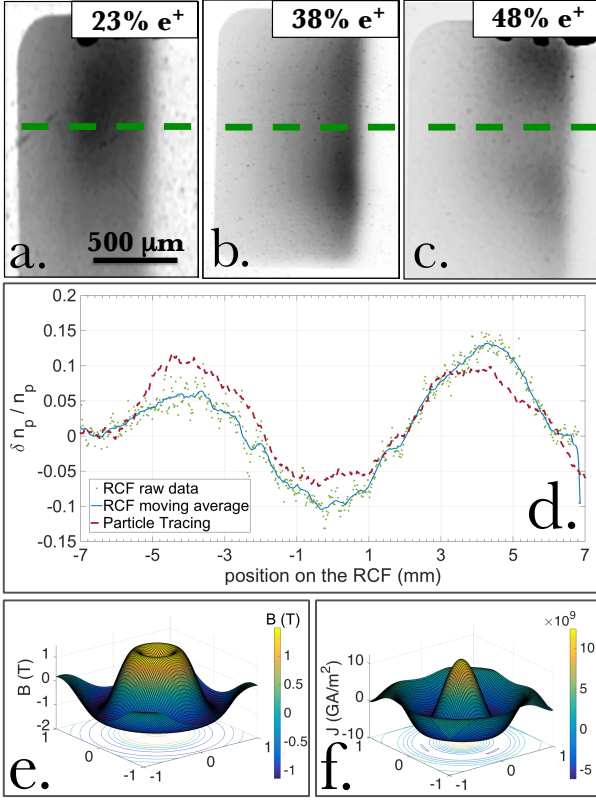


Figure 2. **a.** - **c.** Typical proton radiographies of the background gas after the passage of the electron-positron beam for different percentages of positrons in the beam: 23% (**a.**), 38% (**b.**), and 48% (**c.**). The beam propagates from right to left with the main propagation axis represented by the dashed green line. The spatial scale is common for all frames and refers to the interaction plane. Each radiograph is taken (14 ± 6) ps after the transit of the EPB (corresponding proton energy of 1.1 MeV). The contrast in each image is artificially enhanced for the sake of illustration. **d.** Comparison between the experimental proton distribution (green dots as raw data and solid blue line as a moving average) and the output of the particle-tracing simulation (red dashed curve) for frame **c.** The lineout refers to the detection plane, and the spatial scale is thus magnified by a factor $M \approx 8$. **e.** Distribution of the azimuthal magnetic field used as an input for the particle-tracing simulation and **f.** related current density. Distances are in mm.

these cases, the radiographies show proton accumulation (darker colours on the RCF) on either side of the main EPB propagation axis. It must be noted that, whilst each frame in Fig. 2 refers to a proton energy of 1.1 MeV (probing time of (14 ± 6) ps), radiographies of the same shots at 3.3 MeV and 4.5 MeV (corresponding to probing times of (60 ± 10) ps and (280 ± 30) ps, respectively) show virtually the same deflection patterns, strong indication of the persistence of the fields responsible for the proton deflections. These radiographies are taken long after the EPB has escaped the probed region and we then ascribe

them to magnetic fields left in the background plasma in the wake of the EPB. This conclusion is drawn on the basis that electrostatic fields dissipate on a much shorter time scale, comparable to the inverse plasma frequency of the background plasma (of the order of 100 fs).

In order to extract the magnetic field distribution responsible for the observed proton deflections, Particle Tracing (PT) calculations were performed. The best match with the experimental data is obtained for a magnetic field distribution as shown in Fig. 2.e. Due to the diverging nature of the probing proton beam, the transverse component of the velocity of the probing protons interacts with the azimuthal magnetic field distribution, generating the observed deflections along the vertical axis. This effect is explained in more detail in Ref. [39]. The best match between the PT and the RCF data is obtained for a peak magnetic field of (1.2 ± 0.5) T and a characteristic spatial scale of $\lambda_{\text{fil}} = 1.2 \pm 0.2$ mm (see Figs. 2.d and 2.e). Within the experimental uncertainty, the same magnetic field distribution reproduces the proton deflections also for proton energies of 3.3 and 4.5 MeV, indicating that the magnetic field does not change significantly over the probing temporal window (280 ± 60 ps, corresponding to $(2.5 \pm 0.5) \times 10^3$ inverse plasma frequencies of the background plasma). The current density capable of generating such a magnetic field distribution is shown in Fig. 2.f. As one can see this is made of a positive current density peaking at $J_{\text{max}} \approx 2 \times 10^{10}$ A/m² in the center (corresponding to a particle density of $n_J \approx 2 \times 10^{14}$ cm⁻³), surrounded by a negative current. Given the time-scale of the observation, this corresponds to the return currents left in the background plasma after the propagation of the EPB, which are equal and opposite to the current density structure within the EPB. Given that $n_J \approx n_b$, this is consistent with the EPB creating only one large filamentary structure.

Several numerical [20, 21] and analytical [7, 8] works reported in the literature have discussed the possibility of current filamentation during the propagation of a leptonic beam in a background plasma. In our case, the filamentation instability [40] is expected to generate a transverse modulation with a growth rate of the order of $\Gamma_{\text{fil}} \approx \omega_{p1} \sqrt{(n_b/n_{p1})/\gamma_b} \approx 2 \times 10^{11}$ Hz (growth time of approximately 5 ps). The instability thus takes only 1.5 mm to develop, well within the EPB propagation distance observed in the RCFs. Also the measured wavelength is comparable to twice the beam skin depth, which is of the order of 600 μm.

It must be noted that, for a magnetic field of approximately 1.2 T, the Larmor radius of the background electrons (approximately 30 μm for a simulated background temperature of 10 eV) is much smaller than the typical spatial scale of the magnetic field (of the order of 1 mm), indicating that the background plasma can effectively get magnetised. Moreover, the magnetic field in the background plasma will dissipate only via resistive

effects. This is because collisionless dissipation is ruled out, since the spatial scale of the field is much larger than the skin depth of the background plasma (a few microns). In this regime, the temporal scale for magnetic field dissipation can be estimated as $\tau_{\text{OHM}} \approx \mu_0 \sigma \lambda_{\text{fil}}^2$, with $\sigma = n_e e^2 / (m_e \nu_{ei})$ the classical conductivity of the plasma. For our parameters, the electron-ion collision frequency is of the order of $\nu_{ei} \approx 9 \times 10^8$ Hz, implying a temporal scale for field dissipation of $\tau_{\text{OHM}} \approx 75 \mu\text{s}$. This time is much larger than our observation time, justifying why the field is experimentally seen to retain its shape and amplitude.

In order to test if a beam consisting of equal parts of electrons and positrons can induce a current in the background plasma that is sufficient to sustain a magnetic field with the observed strength, we performed a 2-dimensional Particle-In-Cell (PIC) simulation using the EPOCH code [41]. The simulation box resolves the intervals $0 \leq x \leq 10$ mm along the beam propagation direction and $-1.5 \text{ mm} \leq y \leq 1.5$ mm orthogonal to it by 10^4 grid cells and 3×10^3 grid cells, respectively. We use open boundary conditions for the particles and fields. The pair cloud consists of electrons and positrons with a mean Lorentz factor of $\gamma = 15$. The positron density distribution at the time $t_0 = 0$ is $n_p(x, y, t_0) = f(x) \exp(-y^2/c_p^2)$ with $c_p = 118 \mu\text{m}$. The shape function $f(x) = n_0$ with $n_0 = 10^{16} \text{cm}^{-3}$ if $0 \leq x \leq 30 \mu\text{m}$ and 0 otherwise. The electron density distribution is $n_e(x, y, t_0) = 1.24 f(x) \exp(-y^2/c_e^2)$ with $c_e = 95 \mu\text{m}$. The total number of positrons globally equals that of the electrons but the local net charge imbalance ($c_p \neq c_e$) is purposefully introduced to act as a seed for the instability. The electron-positron cloud is represented by 72 million computational particles (CPs), which are distributed in equal parts over electrons and positrons. The number density of the background electrons is $n_{\text{pl}} = n_0 + 2(n_p - n_e)$ at t_0 and their temperature is 50 eV.

Figure 3 shows the simulation results at the time 16.9 ps and Ref. [42] animates panels (a,b) in time. Figure 3(a) shows the distribution of B_z , which is the out-of-plane component of \mathbf{B} . It shows two bands centered at $y \approx \pm 0.05$ mm where the modulus of B_z is large. The amplitude in the left band is close to zero for $x < 1$ mm and it grows steadily with increasing x . The amplitude oscillates in this band around a mean value that reaches $B_0 = 0.3$ T at $x \approx 4.5$ mm. The oscillation amplitude is comparable to B_0 . The two main bands are surrounded by two weaker magnetic field bands at $y \approx \pm 0.2$ mm. The cumulative charge density of lepton species in Fig. 3(b) oscillates in three bands that separate the bands in Fig. 3(a). Figure 3(c) demonstrates that the driver of the charge density oscillations is the pair cloud. The peak value of the net charge modulus within the contour exceeds the maximum value of $|n_p(x, y, t_0) - n_e(x, y, t_0)|$ by the factor 3; a filamentation-type instability has spa-

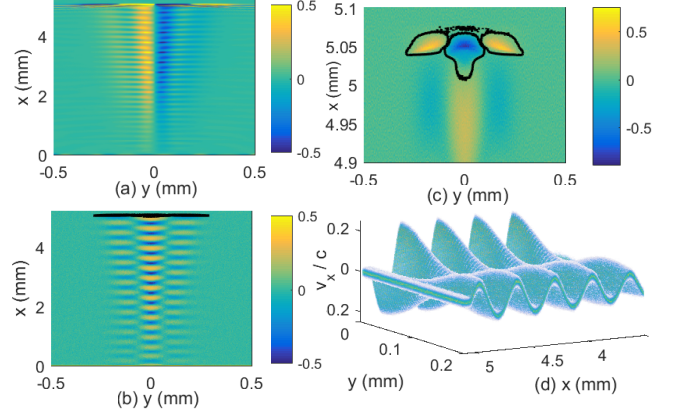


Figure 3. Panel (a) shows the amplitude of $B_z(x, y)$ in units of a Tesla. Panel (b) shows the normalized net charge $(n_p - n_e - n_e)/n_0 + 1$, which takes into account the contribution by the immobile positive background charge. The contour line corresponds to $|n_p - n_e|/n_0 = 0.01$. Panel (c) is a zoom of (b). The phase space distribution $f_b(x, y, v_x)$ of the background electrons is displayed in (d). All the snapshots are taken at a simulated time of $t = 16.9$ ps.

tially separated the cloud's electrons and positrons.

The cloud's propagation along x transforms the temporal growth of its net charge into the observed spatial growth of B_z and of the charge density perturbations in its wake. The velocity oscillations of the background electrons, which are induced by the current of the pair cloud, reach a peak amplitude of $0.25c$ at $y = 0$ in Fig. 3(d), which is the location where the electrons accumulate in the cloud. The latter have a positive mean velocity and they accelerate the background electrons at $x \approx 5$ mm into the opposite direction. The background electrons are accelerated to increasing values of x by the positrons, which gather in Fig. 3(c) at $y \approx \pm 0.2$ mm.

The moving charged pair cloud induces a return current in the background plasma, which explains the observed strong oscillations of B_z and of the net charge density in the wake of the pair cloud. The only stable charge density wave in an unmagnetized plasma with immobile ions is the Langmuir wave. The large oscillation amplitude together with the two-dimensional structure of the currents have resulted in partially magnetic Langmuir oscillations made of an oscillating and a steady state magnetic component.

In conclusion, we report on the experimental evidence of a current-driven instability triggered in a quasi-neutral electron-positron beam as it propagates through a background electron-ion plasma. Experimental data, supported by simple analytical estimates and numerical simulations, provide clear evidence of the generation of strong magnetic fields that persist in the background plasma for thousands of inverse plasma frequencies. This experimental finding is of relevance for the dynamics of lepton-dominated astrophysical jets.

The authors wish to acknowledge support from EPSRC (grants: EP/N022696/1, EP/N027175/1, EP/L013975/1, EP/N002644/1, and EP/P010059/1). The simulations were performed on resources provided by the Swedish National Infrastructure for Computing (SNIC) at HP2CN and on the CINES HPC resource Occigen under the allocation A0010406960 made by DARI/GENCI.

Data sets are available in [URL to be inserted].

-
- [1] R. D. Blandford and R. L. Znajek, *Mon. Not. R. Astron. Soc.* 179, 433 (1977).
 - [2] M. C. Begelman, D. Blandford, and J. Rees, *Rev. Mod. Phys.* 56, 255 (1984).
 - [3] P. Goldreich and W. H. Julian, *Astrophys. J.* 157, 869 (1969).
 - [4] J. F. C. Wardle et al., *Nature* 395, 457 (1998).
 - [5] T. Piran, *Phys. Rep.* 314, 575 (1999).
 - [6] J. L. Racusin et al., *Nature* 455, 183 (2008).
 - [7] A. Bret et al., *Phys. Plasmas* 17, 120501 (2010).
 - [8] M. V. Medvedev and A. Loeb, *Astrophys. J.* 526, 697 (1999).
 - [9] B. Reville et al. *Plasma Phys. Contr. F.* 48, 1741 (2006).
 - [10] Y. Lyubarsky and D. Eichler, *Astrophys. J.* 647, 1250 (2006).
 - [11] A. Gruzinov *Astrophys. J.* 563, 15 (2001).
 - [12] K. M. Ferriere, *Rev. Mod. Phys.* 73, 1031 (2001).
 - [13] T. J. Galama et al., *Nature* 398, 394 (1999).
 - [14] P. M. Vreeswijk et al., *Astrophys. J.* 523, 171 (1999).
 - [15] E. Waxman, *Astrophys. J.* 485, L5 (1997).
 - [16] R. A. M. J. Wijers and T. J. Galama, *Astrophys. J.* 523, 177 (1999).
 - [17] R. Sari et al., *Astrophys. J.* 473, 204 (1996).
 - [18] P. Meszaros et al., *Astrophys. J.* 415, 181 (1993).
 - [19] P. Chang et al., *Astrophys. J.* 674, 378 (2008).
 - [20] P. Muggli et al. *ArXiv: 1306.4380v1* (2013).
 - [21] L. Silva et al. *Astrophys. J.* 596, L121 (2003).
 - [22] M. E. Dieckmann et al. *Astronomy & Astrophysics* 577, A137 (2015).
 - [23] G. Sarri et al., *J. Plasma Phys.* 81, 455810401 (2015).
 - [24] H. Chen et al., *Phys. Rev. Lett.* 114, 215001 (2015).
 - [25] T. S. Pedersen et al. *New J. Phys.* 4, 035010 (2012).
 - [26] E. Liang et al. *Sci. Reports* 5, 13968 (2015).
 - [27] G. Sarri et al., *Nat. Comm.* 6, 6747 (2015).
 - [28] G. Sarri et al., *Plasma Phys. Contr. F.* 55, 124017 (2013).
 - [29] G. Sarri et al. *Phys. Rev. Lett.* 110, 255002 (2013).
 - [30] G. Sarri et al. *New J. Phys.* 12, 045006 (2010).
 - [31] M. Borghesi et al. *Phys. Plasmas* 9, 2214 (2002).
 - [32] C. J. Hooker et al., *J. Phys. IV* 133, 673 (2006).
 - [33] E. Esarey et al., *Rev. Mod. Phys.* 81, 1229 (2009).
 - [34] C. E. Clayton et al., *Phys. Rev. Lett.* 105, 105003 (2010).
 - [35] A. Macchi et al., *Rev. Mod. Phys.* 85, 751 (2013).
 - [36] J. F. Dempsey et al., *Med. Phys.* 27, 2462 (2000).
 - [37] G. Battistoni et al. *AIP conf. proc.* 896, 31 (2007).
 - [38] <http://casinc.com/hyades.html>
 - [39] A. Smyth et al., *Phys. Plasmas* 23, 063121 (2016).
 - [40] K. M. Watson et al., *Phys. Fluids* 3, 741 (1960).
 - [41] T. D. Arber et al., *Plasma Phys. Contr. Fusion* 57, 113001 (2015).
 - [42] See Supplemental Material at [URL will be inserted by publisher] for a time-animation of panels (a) and (b) of Fig. 3 for the times $0.7 \text{ ps} < t < 33.6 \text{ ps}$.